Accepted Manuscript

Geochemistry, $^{40}Ar/^{39}Ar$ geochronology, and geodynamic implications of Early Cretaceous basalts from the western Qinling orogenic belt, China

Feifei Zhang, Yuejun Wang, Peter.A. Cawood, Yunpeng Dong

PII: S1367-9120(17)30570-9
DOI: https://doi.org/10.1016/j.jseaes.2017.10.018
Reference: JAES 3268

To appear in: *Journal of Asian Earth Sciences*

Received Date: 30 November 2016
Revised Date: 30 September 2017
Accepted Date: 16 October 2017

Please cite this article as: Zhang, F., Wang, Y., Cawood, Peter.A., Dong, Y., Geochemistry, $^{40}Ar/^{39}Ar$ geochronology, and geodynamic implications of Early Cretaceous basalts from the western Qinling orogenic belt, China, *Journal of Asian Earth Sciences* (2017), doi: https://doi.org/10.1016/j.jseaes.2017.10.018

Geochemistry, $^{40}Ar/^{39}Ar$ geochronology, and geodynamic implications of Early Cretaceous basalts from the western Qinling orogenic belt, China

Feifei Zhang[a,✉], Yuejun Wang[b], Peter. A. Cawood[c,d], Yunpeng Dong[a]

[a] State Key Laboratory of Continental Dynamics, Department of Geology, Northwest University, Xi'an 710069, China

[b] Guangdong Provincal Key Lab of Geodynamics and Geohazards, School of Earth Sciences and Engineering, Sun Yat-sen University, Guangzhou 510275, China

[c] Department of Earth Sciences, University of St. Andrews, North Street, St. Andrews KY16 9AL, UK

[d] School of Earth, Atmosphere and Environment, Monash University, Melbourne, Victoria 3800, Australia

✉ Corresponding author. Tel.: +86 29 13991110924; E-mail address: zhangff@nwu.edu.cn

Abstract: The Qinling-Dabie orogenic belt was formed by the collision of the North and South China Cratons during the Early Mesozoic and subsequently developed into an intracontinental tectonic process during late Mesozoic. Field investigations identified the presence of late Mesozoic basalts in the Duofutun and Hongqiang areas in the western Qinling orogenic belt. The petrogenesis of these basalts provides an important constraint on the late Mesozoic geodynamics of the orogen. The representative basaltic samples yield the $^{40}Ar/^{39}Ar$ plateau age of about 112 Ma. These samples belong to the alkaline series and have SiO_2 ranging from 44.98 wt.% to 48.19 wt.%, Na_2O+K_2O from 3.44 wt.% to 5.44 wt.%, and MgO from 7.25 wt.% to 12.19 wt.%. They demonstrate the right-sloping chondrite-normalized REE patterns with negligible Eu anomalies (1.00-1.10) and PM-normalized patterns enriched in light rare earth element, large ion lithophile element and high field strength element, similar to those of OIB rocks. These samples additionally show an OIB-like Sr-Nd isotopic signature with $\varepsilon_{Nd}(t)$ values ranging from +6.13 to +10.15 and initial $^{87}Sr/^{86}Sr$ ratios from 0.7028 to 0.7039, respectively. These samples are geochemically subdivided into two groups. Group 1 is characterized by low Al_2O_3 and high TiO_2 and P_2O_5 contents, as well as high La/Yb ratios (>20), being the product of the high-pressure garnet fractionation from the OIB-derived magma. Group 2 shows higher Al_2O_3 but lower P_2O_5 contents and La/Yb ratios (<20) than Group 1, originating from asthenospheric mantle with input of delaminated lithospheric component. In combination with available data, it is proposed for the petrogenetic model of the Early Cretaceous thickened lithospheric delamination in

response to the asthenospheric upwelling along the western Qinling orogenic belt.

Keywords: Basaltic rocks; Early Cretaceous; Geochemical signatures; lithospheric delamination; Western Qinling orogenic belt.

1 Introduction

The Qinling-Dabie orogenic belt was formed by the collision of the North and South China Cratons during the early Mesozoic, which played a fundamental role in the assembly of East Asia (e.g., Mattauer et al., 1985; Kröner et al., 1993; Meng and Zhang, 1999; Zhang et al., 1995, 2001; Ratschbacher et al., 2003; Dong et al., 2011, 2012). Numerous attention has been paid to the early Mesozoic igneous rocks and the metamorphic rocks in the Qinling-Dabie orogenic belt (e.g. Wang et al., 2005; Fan et al., 2004; Wang et al., 2007; Liu et al., 2007; Wang et al., 2014; Hu et al., 2012; Shi et al., 2012), and the collisional process of the North and South China Cratons has been well understood. Available data show that the Dabie orogenic belt had experienced 240-210 Ma collision and deep subduction of continental crust, resulting in the generation of the ultrahigh-pressure metamorphic rocks (e.g. Okay and Sengor 1992; Yin and Nie 1993; Xu et al. 1994; Ernst and Liou 1995; Hacker et al. 1996; Zheng et al. 1998; Zhang et al. 2005; Jiang et al. 2010). The Qinling orogenic belt generally lacks the ultrahigh-pressure rocks with the exception of small amount of blueschists at the Bikou and North Wudang areas (Zhou et al., 1990). In contrast, abundant syn- and post-collisional granites with ages of 245-200 Ma were well developed (Dong et al., 2011a and

references therein), suggestive of Mid-Late Triassic collision along the Mianlue suture zone. Following the collision, this orogenic belt evolved into an intracontinental tectonic process. Our field investigations have identified the presence of late Mesozoic basalts in the western Qinling orogenic belt. These basaltic rocks as the important carriers provide a possibility for probing the source nature and constraining the late Mesozoic geodynamics of the orogen. However, poor attentions have been paid to the late Mesozoic mafic-felsic volcanic rocks erupted in the western Qinling orogenic belt. In this paper, we present a set of petrographical, geochronological and geochemical data of the late Mesozoic basaltic rocks from the western Qinling belt, and aim to probe the intra-continental tectonic process.

2 Geological background

The western Qinling orogenic belt with northwest-southeast extension separates the North China Craton to the northeast from the Yangtze Block of the South China Craton to the southeast, and from the Tibetan Plateau to the southwest (Fig. 1a). It is bounded by the Qinghai Lake–Wushan–Tianshui fault on the north (also known as the West Qinling fault), the A'nyemaqen and Mian-Lue suture zone on the south, and the Wahongshan-Wenquan and Fengxian-Taibai strike-slip faults on the west and east, respectively (Fig. 1b; Feng et al., 2003; Meng et al., 2005; Zhang et al., 2004; Ratschbacher et al., 2003; Dong et al., 2011; Li et al., 2013a).

The Paleozoic to Triassic marine sedimentary package is the oldest exposed sequence in the western Qinling orogenic belt. The Paleozoic rocks are dominated

by shallow-marine carbonate rocks with the exception of the Silurian and Middle to Upper Devonian siltstones and sandstones. The Triassic sequence is composed of deep-marine siliciclastic and carbonate, accumulating in a continental slope environment (Meng et al., 2007). The pre-Jurassic package is overlain by the Jurassic and Cretaceous alluvial and fluvial red-beds (Jiang et al., 2003; Li et al., 2013b; Zhang et al., 2012; Wu et a., 2014). The Middle Jurassic sandstone is overlain by the Lower Cretaceous strata by angular unconformity (Wu et al., 2014).

The western Qinling orogenic belt has experienced strong structural deformation due to the Late Triassic tectonothermal event, as evidenced by folding and thrusting of the Paleozoic-Lower Triassic sequence (Wu et al., 2014). The strike-slip faults and volcanic sequences are important geological signatures during the late Mesozoic. The volcanic sequences are in small volumes and consist mainly of mafic to felsic lava, tuff and volcanic breccia (Ratschbacher et al., 2000; Feng et al., 2002; Zhang et al., 2012). In the central segment of the western Qinling orogenic belt, the volcanic sequence predominantly developed at the Laozanggou, Duofutun and Hongqiang areas (Fig. 1c-d) and constituted a part of the Duofutun and Maixiu groups (Qi et al., 2011). The Duofutun Group with the thickness of 500m consists of basalts, basaltic andesites, andesites, dacites, and rhyolites (Figs. 1c; Qinghai BGMR, 1991; Qi et al., 2011; Li et al., 2013a). The volcanic rocks in the Duohemao Formation of the Maixiu Group are composed of basalts with minor basanites and basaltic andesites (e.g., Fig. 1d; Qinghai BGMR, 1991; Lai et al., 2014; Ding et al., 2013; Qi et al., 2011). The Maixiu Group is unconformably

underlain by the pre-Cretaceous package and unconformably overlain by the Miocene sandy conglomerate. In this study, our samples were collected from the basaltic rocks of the the Duohemao Formation at the Duofutun and Hongqiang areas (Fig. 1). Samples are fresh and display a subaphyric to prophyritic texture with predominant phenocrysts being olivine and pyroxene and the matrix being mainly composed of fine-grained or aphanitic clinopyroxene and plagioclase.

3 Analytical methods

The fresh samples were crushed to millimeter-scale chips and then cleaned in an ultrasonic bath with deionized water. Samples TR-12B and TR-25 were selected for hornblende and whole rock $^{40}Ar/^{39}Ar$ dating analyses, respectively. Whole-rock for Sample TR-25 was hand-picked under a binocular microscope and hornblende for Sample TR-12B was separated by conventional heavy liquid and magnetic techniques. Two samples were irradiated in the central thimble position of the nuclear reactor (1000 kw) at the Chinese Academy of Atomic Energy Science for 2627min with an instantaneous neutron flux of $6.63*10^{12}n/cm^2$. Samples were then heated and degassed in steps from 400–420 °C to 1300 °C. Purified argon was analyzed under MM-1200 mass spectrometer at the Guangzhou Institute of Geochemistry (GIS), the Chinese Academy of Sciences (CAS). The concentrations of ^{36}Ar, ^{37}Ar, ^{38}Ar, ^{39}Ar and ^{40}Ar were corrected for system blank, radioactive decay of nucleonic isotopes, and minor interference reactions involving Ca, K and Cl. The detailed analytical and correction techniques have been described by Sang et al. (1996). The internal standard biotite ZBH-2506 monitor yielded an age of 132.7 ±

1.2 Ma. The $^{40}Ar/^{39}Ar$ dating results were calculated and plotted using the ArArCALC software (Koppers, 2002). The $^{40}Ar/^{39}Ar$ plateau age of the spectra is herein defined by the >75% contiguous gas fractions, at least eight contiguous steps of all the gas evolved from the sample, and their apparent ages agreed to the integrated age of the plateau segment with invariability at 1σ level of uncertainty.

As for representative samples selected for geochemical analyses, rocks chips were powdered to a grain size of 200-mesh by an agate mill. Whole-rock major oxides and trace elemental analyses were performed at the GIG (CAS) by X-ray fluorescence spectrometry and a Perkin-Elmer Sciex ELAN 6000 ICP-MS, respectively. The analytical procedures are described in detail by Li et al. (2002b). Sr and Nd isotopic ratios were measured on the VG-354 mass-spectrometer at the GIG, CAS. Detailed analytical and correction techniques are introduced by Liang et al. (2003). The total procedure blanks were in the range of 200–500 pg for Sr and ⩽50 pg for Nd. $^{86}Sr/^{88}Sr$ ratios and $^{146}Nd/^{144}Nd$ ratios were normalized to 0.1194 and 0.7219, respectively. The measured $^{87}Sr/^{86}Sr$ ratios of the (NIST) SRM 987 standard and $^{143}Nd/^{144}Nd$ ratios of the La Jalla standard are 0.710265 ± 12 (2σ) and 0.511862 ± 10 (2σ), respectively. The elemental and isotopic analytical results are listed in Table 2 and 3, respectively.

4 Results

4.1 Ar-Ar geochronology

The analytical results of TR-12B and TR-25 are shown in Table 1 and Figure 2. Hornblende grains for TR-12B yield a plateau age of 112 ± 0.6 Ma defined by ~99 %

released gas (Fig. 2a). The plateau age is comparable with its isochron age, and the initial $^{40}Ar/^{39}Ar$ ratio is 267.49, suggesting an insignificant excess of ^{40}Ar or ^{36}Ar. Whole- rock sample (TR-25) gives a plateau age of 112.0 ± 2.3 Ma with 92.4% ^{39}Ar released gas (Fig. 2b). Its plateau age is consistent with the isochron ages, with a correlation coefficient of 0.994, indicative of a reliable plateau age.

4.2 Geochemical results

The Early Cretaceous basaltic samples are geochemically subdivided into two groups. Group 1 is constituted by four samples from the Duofutun area (TR-5, TR-7, TR-9 and TR-11), which is characterized by low Al_2O_3 (12.23-12.66 wt.%) and high TiO_2 (2.69-2.87 wt.%) and P_2O_5(0.72-0.81 wt.%) contents. It gives high La/Yb ratios (>20). Group 2 from the Duofutun and Hongqiang areas shows higher Al_2O_3 (14.05-16.48 wt.%) and lower P_2O_5 (0.41-0.67 wt.%) contents and La/Yb ratios (<20) than those of Group 1.

On the plot of total alkali and SiO_2 (Fig. 3), both groups have typical alkaline series and plot into the basalt field with the exception of two samples (TR-2 and TR-3) in the trachy-basalt field. On Harker diagrams, these samples are decreasing in CaO, TiO_2, P_2O_5, and FeOt contents but slightly varying in MgO and Al_2O_3 contents with increasing SiO_2 (Fig. 4a-f). The compatible elements (e.g. Cr and Ni) positively correlated with MgO (Fig. 4g-h). Group 1 has higher Nb and La contents (61.93-71.93 and 36.63-40.12, respectively) than Group 2 (28.03-55.39 and 18.24-33.51, respectively).

Both groups show similar chrondrite-normalized REE patterns with enrichment

in LREE ((La/Yb)n=7.07–19.48) and insignificant Eu anomalies (1.00-1.10), resembling to those of typical ocean island basalt (Fig. 5a; Sun and McDonough, 1989). The Group 1 sampes has higher LREE/HREE ratios and more insignificant Eu anomalies than the Group 2. On the primitive mantle- normalized spidergrams (Fig. 5b), the Group 1 and 2 samples show OIB-like patterns (Sun and McDonough, 1989) with enrichment in LREE, LILE and HFSE but relative depletion in HREE. The positive Nb, Ta and Sr but negative Rb anomalies are additionally shown. La/Nb ratios range from 0.56 to 0.70, Ba/La from 4.99 to 21.9 and Ba/Nb from 2.94 to 12.4, similar to those of oceanic island basalt (0.77, 9.49 and 7.29, respectively; Sun and McDonough, 1989).

The Sr and Nd isotopic compositions for the thirteen samples are listed in Table 2 and Figure. 6. Two samples from Group 1 are analyzed for Sr and Nd isotopic compositions and have initial $^{87}Sr/^{86}Sr$ ratios of 0.7039 and $\varepsilon_{Nd}(t)$ values of +6.13 - +7.37 respectively, similar to those of the OIB rocks. Group 2 has the measured $^{87}Sr/^{86}Sr$ ratios of 0.7028-0.7036 and $^{143}Nd/^{144}Nd$ ratios of 0.5130-0.5131, falling within the MORB and/or OIB fields. Group 2 exhibits lower initial $^{87}Sr/^{86}Sr$ ratios (0.7028 - 0.7035) and higher $\varepsilon_{Nd}(t)$ values (+7.36 - +10.15) than Group 1. Our Group 1 and 2 samples have lower $^{87}Sr/^{86}Sr$ but higher $^{143}Nd/^{144}Nd$ ratios than those of Cenozoic basalts in East China (Fig. 6).

5 Discussion

5.1 Low temperature alteration

The relatively high loss on ignition (LOI) of these samples raises the possibility

that the basaltic samples might have undergone post-eruption alteration. Some incompatible elements, e.g., Rb and Ba, are known to be mobile during weathering (Deniel, 1998), and show considerable variation in Figure 5b. However, the similar primitive-mantle normalized pattern for the majority of the incompatible elements (except Rb and Ba) suggests an insignificant low-temperature alteration. In addition, there is insignificant correlation between LOI and Sr-Nd isotopic compositions (not shown), further suggesting a negligible effect of low temperature alteration (Jochum et al., 1991; Deniel, 1998; Kerrich et al., 1999; Xu et al., 2001; Wang et al., 2004). Accordingly, the following discussion focuses on the immobile elements and Sr-Nd isotopic composition.

5.2 Fractional crystallization and crustal contamination

It is difficult to evaluate the role of fractionation crystallization for the Group 1 samples due to their narrow compositional range. However, their low mg-numbers and compatible elemental contents might be indicative of significant differentiation. For the Group 2 samples, increasing Ni and Cr with increasing MgO (Fig. 4g-h) suggests the crystallization fractionation of olivine and clinopyroxene. This is also in accordance with the decrease FeO_t and CaO and increasing SiO_2 (Fig. 4a-c). Fractional crystallization of plagioclase is most likely Insignificant, as suggested by the insignificant Eu anomalies (Fig. 5a). The negative correlations of SiO_2 with TiO_2 and P_2O_5 could have resulted from the fractionation of apatite and Ti-Fe-oxides. However, a simple fractionation model cannot explain the variable concentration of incompatible elements and poor correlation of SiO_2 and MgO and Al_2O_3.

Crustal contamination for mantle-derived magma is a potential process since the mafic magma would transit through continental crust prior to eruption. Crust-derived magma has generally higher Th/La and lower Nb/La ratios relative to mantle-derived magma (Rudnick and Gao, 2003). The Group 1 have higher Nb/La ratios and TiO_2 and FeOt contents than those of average continental crust (Rudnick and Fountain, 1995). They additionally exhibit an insignificant correlation between SiO_2 and Th/La and Nb/La. Such signatures query the significant crustal assimilation or AFC processes for the magma (e.g., DePaolo, 1981).

The Group 2 exhibits a positive correlation between SiO_2 and Th/La ratios (Fig. 7a) and increasing $(^{87}Sr/^{86}Sr)_i$ ratios and decreasing $\varepsilon_{Nd}(t)$ values with increasing SiO_2 (Fig. 7c-d). Such signatures suggest to some degree crustal contamination of mantle-derived magma. However, the analyzed samples have relatively high $\varepsilon_{Nd}(t)$ values and low $(^{87}Sr/^{86}Sr)_i$ ratios (Table 3 and Fig. 6). In addition, Sample TR-12(B) and TR-13 have the lowest $\varepsilon_{Nd}(t)$ values but relatively higher mg-numbers, contradictive to the crustal assimilation and the assimilated fractionation processes. In Figure 5b, our samples have insignificant Nb, Ta, P and Ti depletion. In Fig.8, they plot along the partial melting and/or source heterogeneity evolved trend. These characteristics synthetically suggest the source heterogeneity being the main control factor for Group 1 and 2.

5.3 Source characteristics

The varied LILE and HFSE contents for the Group 2 might be interpreted as the result of variable-degree partial melting of the mantle source. However, the ratios of

highly incompatible elements with similar bulk distribution coefficients (e.g.Nb/U) are relatively constant during partial melting. The Group 2 have Nb/U of 27.8-67.9, suggestive of their derivation from a heterogeneous source.

The Group 2 has relatively high $(La/Yb)_n$ ratios of 7.35 - 13.32 and Sr/Y ratios of 27.39 - 46.90, but low Lu/Hf ratios of 0.05 - 0.08 (Table 2) and show the OIB-like multi-elemental patterns with enrichment in LILE, HFSE and LREE, as well as insignificant Nb-Ta anomalies (Fig. 5a-b; McDonough et al., 1985; Tibaldi et al., 2008). Nb/U and Ba/Ce ratios range from 27.8 to 67.9 and 2.45 to 10.71, respectively (Halliday et al., 1995). These ratios, along with low $(^{87}Sr/^{86}Sr)_i$ ratios and high $\varepsilon_{Nd}(t)$ values, are similar to those of an OIB-derived magma (Figs. 5b and 6; Halliday et al., 1995; Sun and McDonough, 1989). The LREE/HREE fractionation in the alkaline basalts might be explained as the melting result of metasomatized amphibole-bearing lithosphere. Zr/Nb ratios positively correlated to Ce/Y ratios in response to the partial melting of an amphibole-bearing spinel or garnet lherzolite. However, negative correlation of La/Yb with Dy/Yb is shown when the spinel lherzolite source is partially melting (Beker et al., 1997). The absence of such correlations for our samples argues against the petrogenetical possibility. Therefore, it is inferred that the OIB-like alkaline volcanic rocks generated from an asthenospheric source, further evidenced by their low HFSE/LREE ratios. The Group 2 displays lower $^{143}Nd/^{144}Nd$ and higher $^{87}Sr/^{86}Sr$ ratios relative to depleted mantle, plotting into the Hawaii OIB field in Figure 6. The Sr-Nd isotopic systematics is distinct from that of the Cenozoic basalts in East China (e.g. Zou et al, 2000; Liu et al., 1996). The depleted Sr-Nd isotopic compositions for

Group 2 plot in the field near to FOZO (Hart et al. 1992 and Stracke et al. 2005), indicative of involvement of FOZO-like component in the magma source. As shown in Figs. 7a-d, the Group 2 samples define a binary mixing array of the asthenospheric with FOZO end members, as shown in Fig. 6.

The Group 1 samples have relatively high $(La/Yb)_n$ and Sr/Y but low Lu/Hf ratios. They show OIB-like multi elemental patterns, similar to Group 2 samples. The Group 1 samples additionally show higher TiO_2, P_2O_5 and La contents, and La/Yb (>20) and Sm/Yb ratios, as well as lower HREE contents than the Group 2 samples (e.g. Deniel, 1998; Xu et al., 2001; Zhou et al., 2006). The crystallization fractionation of garnet with clinopyroxene can result in the increasing Sm/Yb and LREE/HREE ratios and TiO_2 contents, as observed in the Longhai basalts in East China (Zeng et al., 2017; Klemme et al., 2002; Pertermann et al., 2004). As a result, the Group 1 samples might be the product of fractionation crystallization of garnet and clinopyroxene for asthenosphere-derived magma (Fig. 8).

5.4 Tectonic implications

The basaltic samples in the western Qinling orogenic belt occurred mainly within Mesozoic sedimentary basins, which are spatially associated with syn-deposited faulting (Qinghai BGMR, 1991). Our representative samples give the $^{40}Ar/^{39}Ar$ age of ~112 Ma. Li et al. (2013a) reported the $^{40}Ar/^{36}Ar$ plateau age of 103 ± 2 Ma and zircon U-Pb ages of 106 ± 1 Ma and 101 ± 1 Ma for the Duofutun basalt. Ding et al. (2013) reported the zircon U-Pb dating age of 105 ± 1 Ma for the Hongqiang alkaline basalts. These data indicate that the basaltic rocks erupted at Early

Cretaceous. As mentioned above, these basaltic samples show typical alkaline affinity with low SiO_2 and Al_2O_3 contents and high TiO_2 and Na_2O/K_2O ratios (>1) (e.g., Feng et al., 2002; Li et al., 2013a; Ding et al., 2013; Qi et al., 2011), suggesting the derivation of asthenospheric source with input of FOZO-like component.

A FOZO-like component has been commonly thought to relate to the mantle plume (e.g., Siebel et al., 2000; Bertrand et al., 2003). However, the Late Mesozoic hotspot track and related geological evidence have not been observed in the western Qinling orogenic belt. It is an alterative for the FOZO-like component in the depleted mantle source being petrogenetically related to the delaminated lithospheric mantle (Stracke et al., 2005). Available data show that the intermediate-acidic volcanic rocks at Longzanggou near Duofutun area (Fig. 1c) erupted at 128-130 Ma ($^{40}Ar/^{39}Ar$ age) and are characterized by andesites-dacites (Zhang et al, unpublished data). In comparison with the basaltic rocks at the Duofutun and Hongqiang areas, these intermediate-acidic volcanic rocks show the calc-alkaline geochemical characteristics with enrichment in LILE and LREE and depletion in HFSE, suggestive of a mantle source with input of enriched lithospheric component. As a result, the Early Cretaceous volcanic rocks in the western Qinling belt show a compositional variation from intermediate-acidic calc-alkaline andesites-dacites at ~130 Ma to alkaline basalts at ~110 Ma. Such a trend in composition probably suggests the involvement of the detachment lithosphere, which results from the gravitational instability following the crustal shortening (e.g.,

Schott et al., 2000; Molnar et al., 1998). In the western Qinling orogenic belt, there developed the pre-Cretaceous transpressive structures (e.g., folds, faults and sheets; Dong et a., 2011, 2015, 2016), the angular unconformity between the upper Cretaceous and pre-Cretaceous sequences (e.g., Qinghai BGMR, 1991; Wu et al., 2014), and a Late Jurassic compression deformation in the Huicheng basin (Li et al., 2013b). These geological signatures suggest the development of the crustal shortening prior to the basalt eruption, probably at the Late Jurassic-Early Cretaceous period. Following the crustal shortening, the thickened lithospheric root was removed and the hot asthenospheric mantle uplift. In response to the asthenospheric upwelling (Gao et al., 2004; Hoernle et al., 2006), the softing and decompression melting of lithospheric mantle generated the ~130 Ma intermediate-acidic volcanic rocks. And then the interaction of the upwelling asthenospheric with lithospheric source was contributed to the ~110 Ma basaltic rocks in the western Qinling orogenic belt.

6 Conclusions

Based on our $^{40}Ar/^{39}Ar$ geochronological results, along with whole-rock elemental and Sr–Nd isotopic data for the basalts from the Duofutun and Hongqiang areas in the western Qinling orogenic belt, the following conclusions can be outlined.

(1) The representative basaltic samples from the Duofutun area yield the $^{40}Ar/^{39}Ar$ age of ~112 Ma, suggesting a magmatic event in the western Qinling orogenic belt during the Early Cretaceous.

(2) These samples are alkaline basalts with OIB-like geochemical signatures. They can geochemically be subdivided into two groups with Group 1 being the product of the high-pressure garnet fractionation of mantle-derived magma and Group 2 originating from asthenosphere with an input of the delaminated lithospheric component.

(3) The generation of the Early Cretaceous basalts was goedynamically related to the thickened lithospheric delamination in the asthenspheric upwelling setting along the western Qinling orogenic belt.

Acknowledgements

The authors would like to thank Dr. X.Y. Li and L.Y. Fan for their help in sample collection. This work was financially supported by Chinese National Natural Science Foundation (Grants. 41421002, 41302176 and 41190074), National Basic Research Program of China (2016YFC0600303 and 2014CB440901) and Foundation of Shaanxi Educational committee (14JK1760). P.A. Cawood acknowledges support from Australian Research Council (Grant FL160100168).

References

Ayers, J.C., Dunkle, S., Gao, S., Miller, C.F., 2002. Constraints on timing of peak and retrograde metamorphism in the Dabie Shan Ultrahigh-Pressure Metamorphic Belt, east-central China, using U-Th-Pb dating of zircon and monazite. Chem. Geol. 186, 315–331.

Bertrand, H., Chazot, G., Blichert-Toft, J., Thoral, S., 2003. Implications of widespread high-μ volcanism on the Arabian Plate for Afar mantle plume and lithosphere composition. Chem. Geol. 198, 47–61.

Campbell, I.H., 2005. Large igneous provinces and the mantle plume hypothesis. Elements 1, 265–270.

Chase, C.G., 1981. Oceanic island Pb: two-stage histories and mantle evolution. Earth Planet. Sci. Lett. 52, 277–284.

Chauvel, C., Hofmann, A.W., Vidal, P., 1992. HIMU-EM: the French Polynesia connection. Earth Planet. Sci. Lett. 110, 99–119.

Courtillot, V., Davaille, A., Besse, J., Stock, J., 2003. Three distinct types of hotspots in the Earth's mantle. Earth Planet. Sci. Lett. 205, 295–308.

Courtillot, V., Jaupart, C., Manighetti, I., Tapponier, P., Besse, J., 1999. On causal links between flood basalts and continental breakup. Earth Planet. Sci. Lett. 166, 177–195.

Craddock, W.H., Kirby, E., Zheng D.W., Liu J.H., 2012. Tectonic setting of Cretaceous basins on the NE Tibetan Plateau: insights from the Jungong Basin. Basin Res. 24, 51–69.

DePaolo, D.J., Daley, E.E., 2000. Neodymium isotopes in basalts of the Southwest Basin and Range and lithospheric thinning during continental extension. Chem. Geol. 169, 157–185.

DePaolo, D.J., 1981. Trace element and isotopic effects of combined wall rock assimilation and fractional crystallization. Earth Planet. Sci. Lett. 53, 189–202.

Ding, Y., Yu, X.H., Mo, X.X., Li, X.W., Huang, X.F., Wei, P., 2013. Geochronology, geochemistry and petrogenesis of the Hongqiang basalts from Northeast Qinghai-Tibetan Plateau. Earth Sci. Frontiers 20, 180–191 (in Chinese with English Abstract).

Dong, Y., Genser, J., Neubauer, F., Zhang, G., Liu, X., Yang, Z., Heberer, B., 2011. U–Pb and $^{40}Ar/^{39}Ar$ geochronological constraints on the exhumation history of the North Qinling terrane, China. Gondwana Res. 19, 881–893.

Ernst, W.G., Liou, J.G., 1995. Contrasting platetectonic styles of the Qinling–Dabie–Sulu and Franciscan metamorphic belts. Geology, 23, 353–356.

Fan, W.M., Guo, F., Wang, Y.J., Zhang, M., 2004. Late Mesozoic volcanism in the northern Huaiyang tectono-magmatic belt, central China: partial melts from a lithospheric mantle with subducted continental crust relicts beneath the Dabie Orogen? Chem. Geol. 209 (1–2), 27–48.

Farmer, G.L., 2003. Continental basaltic rocks. Treatise on Geochemistry, Elsevier Pergamon, Oxford, pp, 85–121.

Feng, Y.M., Cao, X.D., Zhang, E.P., Hu, Y.X., Pan, X.P., Yang, J.L., Jia, Q.Z., Li, W.M., 2003. Tectonic Evolution framework and nature of the West Qinling orogenic belt. Northwestern Geol. 36, 1–10 (in Chinese with English abstract).

Feng, Y.M., Gao, X.Z., Zhang, E.P., Hu, Y.X., Pan, X.P., Yang, J.L., Jia, Q.Z., Li, W.M., 2002. Structure, orogenic processes and geodynamic of the western Qinling orogen. Xi'an Map Press, Xi'an, pp. 1–263, (in Chinese).

Fitton, J.G., James, D., Leeman, W.P., 1991. Basic magmatism associated with Late

Cenozoic extension in the western United States: compositional variations in space and time. J. Geophys. Res. 96, 13693–13711.

Gao, S., Rudnick, R.L., Yuan, H.L., Liu, X.M., Liu, Y.S., Xu, W.L., Ling, W.L., Ayers, J., Wang, X.C., Wang, Q.H., 2004. Recycling lower continental crust in the North China Craton. Nature 432, 892–897.

Hart, S.R., Hauri, E.H., Oschmann, L.A., Whitehead, J.A., 1992. Mantle plumes and entrainment: isotopic evidence. Science 256, 517–520.

Hauri, E.H., Whitehead, J.A., Hart. S.R., 1994. Fluid dynamic and geochemical aspects of entrainment in mantle plumes, J. Geophys. Res. 99, 24275–24300.

Hacker, B.R., Ratschbacher, L.W., Ireland, L., Walker, D., Dong, S., 1998. U/Pb zircon ages constrain the architecture of the ultrahigh-pressure Qinling-Dabie Orogen, China. Earth Planet. Sci. Lett. 161, 215– 230.

Halliday, A.N., Lee, D.-C., Tommasini, S., Davies, G.R., Paslick, C.R., Fitton, J.D., James, D.E., 1995. Incompatible trace elements in OIB and MORB and source enrichment in the sub-oceanic mantle. Earth Planet. Sci. Lett. 133, 379–395.

Hirose, K., Kushiro, I., 1993. Partial melting of dry peridotites at high pressures: determinations of compositions of melts segregated from peridotite using aggregates of diamond. Earth Planet. Sci. Lett. 114, 477–489.

Hoernle, K., White, J.D.L., van den Bogaard, P., Hauff, F. Coombs, D.S., Werner, R., Timm, C., GarbeSchönberg, D., Reay, A., Cooper, A.F., 2006. Cenozoic intraplate volcanism on New Zealand: Upwelling induced by lithospheric removal. Earth Planet. Sci. Lett. 248, 350–367.

Hofmann, A.W., 2004. Sampling mantle heterogeneity through oceanic basalts: isotopes and trace elements. In: Carlson, R.W. (Ed.), The Mantle and Core, Treatise in Geochemistry. Elsevier, Amstredam, pp. 61–103.

Hu, J.M., Chen, H., Qu, H.J.,Wu, G.L., Yang, J.X., Zhang, Z.Y., 2012. Mesozoic deformations of the Dabashan in the southern Qinling orogen, central China. J. Asian Earth Sci. 47, 171–184.

Jahn, B.M., Wu, F.Y., Lo, C.H., Tsai, C.H., 1999. Crust– mantle interaction induced by deep subduction of the continental crust: Geochemical and Sr–Nd isotopic evidence from post-collisional mafic–ultramafic intrusions of the northern Dabie complex, central China. Chem. Geol. 157, 119– 146.

Jiang, Y.H., Jin, G.D., Liao, S.Y., Zhou, Q., Zhao, P., 2010. Geochemical and Sr–Nd–Hf isotopic constraints on the origin of Late Triassic granitoids from the Qinling orogen, central China: implications for a continental arc to continent–continent collision. Lithos 117, 183–197.

Jochum, K.P., Arndt, P.N.T., Hofmann, A.W., 1991. Nb–Ta-La in komatiites and basalts: constraints on komatiite petrogenesis and mantle evolution. Earth Planet. Sci. Lett. 107, 272–289.

Kerrich, R., Polat, A., Wyman, D., Hollings, P., 1999. Trace element systematics of Mg- to Fe-tholeiitic basalt suites of the Superior Province: implications for Archean mantle reservoirs and greenstone belt genesis. Lithos 46, 163–187.

Klemme, S., Blundy, J.D., Wood, B.J., 2002. Experimental constraints on major and trace element partitioning during partial melting of eclogite, Geochim.

Cosmochim. Acta 66, 3109–3123.

Koppers, A.A.P., 2002. ArAR CALC- software for 40Ar/39Ar age calculations. Comput.& Geosci. 28, 605–619.

Kröner, A., Zhang, G.W., Sun, Y., 1993. Granulitesin the Tongbai area, Qinling belt, China: geochemistry, petrology, single zircon geochronology, and implications for the tectonic evolution of eastern Asian. Tectonics 12, 245–255.

Kushiro, I., 2001. Partial melting experiments on peridotite and origin of mid-ocean ridge basalts. Annu. Rev. Earth Planet. Sci. 29, 71–107.

Lai, S.C, Qin, J.F., Khan, J., 2014. The carbonated source region of Cenozoic mafic and ultra-mafic lavas from western Qinling: Implications for eastern mantle extrusion in the northeastern margin of the Tibetan Plateau. Gondwana Res. 25, 1501–1516.

Langmuir, C.H., Klein, E.M., Plank, T., 1992. Petrological systematics of mid-ocean ridge basalts: constraints on melt generation beneath ocean ridge. American Geophysical Union Geophysical Monograph Series 71, 81–180.

Le Maitre, R.W., 2002. Igneous Rocks: A Classification and Glossary of Terms, Second edition. Cambridge University Press, Cambridge.

Li, W., Dong, Y.P., Guo, A.L., Liu, X.M., Liu, Y.Q., Zha, X.F., Zhang, K.L., 2013b. Sedimentary fill history of the Huicheng Basin in the West Qinling Mountains and associated constraints on Mesozoic intracontinental tectonic evolution. Sci. China Earth Sci. 43 (5), 730–744.

Li, X.H., Li, Z.X., Zhou, H., Liu, Y., Kinny, P.D., 2002. U–Pb zircon geochronology,

geochemistry and Nd isotopic study of Neoproterozoic bimodal volcanic rocks in the Kangdian Rift of South China: implications for the initial rifting of Rodinia. Precambrian Res. 113 (1–2), 135–154.

Li, X.W., Mo, X.X., Yu, X.H., Ding, Y., Huang, X.F., Wei, P., He, W.Y., 2013a. Geochronological, geochemical and Sr–Nd–Hf isotopic constraints on the origin of the Cretaceous intraplate volcanism in West Qinling, Central China: Implications for asthenosphere–lithosphere interaction. Lithos 177, 381–401.

Liang, X.R., Wei, G.J., Li, X.H., Liu, Y., 2003. Precise measurement of 143Nd/144Nd and Sm/Nd ratios using multiple-collectors inductively couple plasma-mass spectrometer (MC-ICP-MS). Geochimica 32 (1), 91–96 (in Chinese with English abstract).

Liu, C.Q., Xie, G.H., Akimasa, M., 1995. Geochemistry of Cenozoic basalts from eastern China: (II) Sr, Nd, and Ce isotopic compositions. Geochimica 24(3), 203-214 (in Chinese with English abstract).

Mattauer, M., Matte, Ph., 1985. Tectonics of the Qinling Belt: build-up and evolution of eastern Asia. Nature, 317, 196–500.

McBirney, A.R., 1993. Igneous petrology. Jones and Bartlett Publishers, London, UK. 508.

McDonough, W.F., McCulloch, M.T., Sun, S.S., 1985. Isotopic and geochemical systematic in Tertiary–Recent basalts from southeastern Australia and implications for the evolution of the sub-continental lithosphere. Geochim. Cosmochim. Acta 49, 2051–2067.

Meng, Q., Qu, H., Hu, J., 2007. Triassic deep-marine sedimentation in the western Qinling and Songpan terrane. Sci. China Earth Sci. 50 (Suppl. II), 246–263.

Meng, Q., Zhang, G.W., 1999. Timing of the collision of the North and South China Blocks: controversy and reconciliation. Geology, 27, 123–126.

Meng, Q.R., Wang, E., Hu, J.M., 2005. Mesozoic sedimentary evolution of the northwest Sichuan basin: implication for continued clockwise rotation of the South China block. Geol. Soc. Am. Bull. 117, 396–410.

Molnar P., Houseman G. A., and Conrad C., 1998. Rayleigh–Taylor instability and convective thinning of mechanically thickened lithosphere: effects of nonlinear viscosity decreasing exponentially with depth and of horizontal shortening of the layer. Geophys. J. Int. 133, 568–584.

Nicholson, H., Latin, D., 1992. Olivine tholeiites from Krafla, Iceland: evidence for variations in the melt fraction within a plume. J. Petrol. 33, 1105–1124.

Niu, Y., O'Hara, M.J., 2003. Origin of the ocean island basalts: a new perspective from petrology, geochemistry, and mineral physics considerations. J. Geophys. Res. 108 (B4), 2209.

Okay, A.I., Sengor, A.M.C., 1992. Observations for intracontinental thrust-related exhumation of ultrahigh- pressure rocks in China. Geology 20, 411–414.

Pertermann, M., Hirschmann, M.M., Hametner, K., Günther, D., Schmidt, M.W., 2004. Experimental determination of trace element partitioning between garnet and silica-rich liquid during anhydrous partial melting of MORB-like eclogite, Geochem. Geophys. Geosyst., 5, Q05A01, doi:10.1029/2003GC000638.

Pilet, S., Hernandez, J., Sylvester, P., Poujol, M., 2005. The metasomatic alternative for ocean island basalt chemical heterogeneity. Earth Planet. Sci. Lett. 236, 148–166.

QBGMR (Qinghai Bureau of Geology and Mineral Resources), 1991. Regional Geology of Qinghai Province. Geology Publishing House, Beijing, 662 (in Chinese).

Qi, S.S., Deng, J.F., Zhao, C.X., Hu, X.L., Shi, L.C., Chen, J., 2011. The evidence for the existence of Early Cretaceous continental rift in West Qinling orogenic belt: the significance of the newly built Maixiushan Group in Tongren area of Qinghai Province. Geological Bulletin of China 30, 1706-1715.

Ratschbacher, L., Hacker, B.R., Calvert, A., Webb, L.E., Grimmer, J.C., McWilliams, M.O., Ireland, T., Dong, S., Hu, J., 2003. Tectonics of the Qinling (Central China): tectonostratigraphy, geochronology, and deformation history. Tectonophysics 366, 1–53.

Rudnick, R.L., Gao, S., 2003. Composition of the continental crust. In: Rudnick, R.L. (Ed.), Treatise on Geochemistry, vol. 3, The Crust. Elsevier, pp. 1–64.

Rudnick, R.L., Fountain, D.M., 1995. Nature and composition of the continent-crust: a lower crustal perspective. Rev. Geophys. 33 (3), 267–309.

Sang, H.Q., Wang, S.S., Qiu, J., 1996. The ^{40}Ar–^{39}Ar ages of pyroxene, hornblende and plagioclase in Taipingzhai granulites in Qianxi County, Hebei Province and their geological implications. Acta Petrol. Sin. 12 (4), 390–400 (in Chinese with English abstract).

Schott, B. Yuen, D.A., Schmeling, H., 2000. The significance of shear heating in continental delamination, Phys. Earth Planet. Inter. 118, 273–290.

Shi, W., Zhang, Y., Dong, S., Hu, J., Wiesinger, M., Ratschbacher, L., Jonckheere, R., Li, J., Tian, M., Chen, H., Wu, G., Ma, L., Li, H., 2012. Intra-continental Dabashan orocline, southwestern Qinling, Central China. J. Asian Earth Sci. 46, 20–38.

Siebel,W., Becchio, R., Volker, F., Hansen, M.A.F., Viramonte, J., Trumbull, R.B., Haase, G., Zimmer, M., 2000. Trindade and Martin Vaz Islands, South Atlantic: isotopic (Sr–Nd–Pb) and trace element constraints on plume related magmatism. J. S. Am. Earth. Sci. 13, 79–103.

Smith, E.I., Sánchez, A., Walker, J.D., Wang, K., 1999. Geochemistry of mafic magmas in the Hurricane Volcanic Field, Utah: implications for small- and large scale chemical variability of the lithospheric mantle. J. Geol. 107, 433–448.

Stracke, A., Hofmann, A.W., Hart, S.R., 2005. FOZO, HIMU and the rest of the mantle zoo. Geochem. Geophys. Geosyst. 6 (5), Q05007. doi:10.1029/ 2004GC000824.

Sun, S.S., McDonough, W.F., 1989. Chemical and isotopic systematics of oceanic basalts: implications for mantle composition and processes. In: Saunders, A.D., and Norry, M.J., (eds) Magmatism in the Ocean Basins. Geological Society, London, Special Publications 42, 313–345.

Takahashi, E., Kushiro, I., 1983. Melting of a dry peridotite at high pressures and basalt magma genesis. Am. Mineral. 68, 859–879.

Tibaldi, A.M., Otamendi J.E., Gromet, L.P., Demichelis, A.H., 2008. Suya Taco and Sol de Mayo mafic complexes from eastern Sierras Pampeanas, Argentina: Evidence for the emplacement of primitive OIB-like magmas into deep crustal levels at a late stage of the Pampean orogeny. J. S. Am. Earth. Sci. 26, 172–187.

Wang, F., Zhu, R.X., Hou, Q.L., Zheng, D.W., Yang, L.K., Wu, L., Shi, W.B., Feng, H.L., Sang, Q.H., Zhang, H.Y., Liu, Q., 2014. $^{40}Ar/^{39}Ar$ Thermo-chronology on Central China Orogen: Cooling, uplift and implications for orogeny dynamics. Jourdan, F., Mark, D. F. & Verati, C. (eds) 2014. Advances in $^{40}Ar/^{39}Ar$ Dating: from Archaeology to Planetary Sciences. Geological Society, London, Special Publications, 378, 189–206.

Wang, Y.J., Fan, W.M., Peng, T.P., Zhang, H.F., Guo, F., 2005. Nature of the Mesozoic lithospheric mantle and tectonic decoupling beneath the Dabie Orogen, Central China: evidence from $^{40}Ar/^{39}Ar$ geochronology, elemental and Sr–Nd–Pb isotopic compositions of Early Cretaceous mafic igneous rocks. Chem. Geol. 220, 165–189.

Wang, Y.J., Fan, W.M., Zhang, Y.H., Guo, F., Zhang, H.F., Peng, T.P., 2004. Geochemical, $^{40}Ar/^{39}Ar$ geochronological and Sr–Nd isotopic constraints on the origin of Paleoproterozoic mafic dikes from the southern Taihang Mountains and implications for the ca. 1800 Ma event of the North China Craton. Precambrian Res. 135, 55–77.

Weaver, B.L., 1991. Trace element evidence for the origin of ocean–island basalts.

Geology 19, 123–126.

Wu, G.L., Meng, Q.R., Duan, L., Li, L., 2014. Early Mesozoic structural evolution of the eastern West Qinling, northwest China. Tectonophysics 630, 9–20.

Xu, S., Liu, Y.C., Jiang, L.L., Su, W., Ji, S.Y., 1994. Tectonic framework and evolution of Dabieshan. Science Press, Beijing. (in Chinese with English abstract).

Xu, Y.G., Chung, S.L., Jahn, B.M., Wu, G.Y., 2001. Petrologic and geochemical constraints on the petrogenesis of Permian- Triassic Emeishan flood basalts in southwestern China. Lithos 58, 145–168.

Yin, A., Nie, S., 1993. An indentation model for the North and South China collision and the development of the Tanlu and Honam fault systems, eastern Asia. Tectonics 12, 801–813.

Zeng, G., Chen, L.H., Yu, X., Liu, J.Q., Xu, X.S., Erdmann, S., 2017. Magma-magma interaction in the mantle beneath eastern China. J. Geophys. Res. Solid Earth, 122, doi:10.1002/2017JB014023.

Zindler, A., Hart, S., 1986. Chemical geodynamics. Annu. Rev. Earth Planet. Sci. 14, 493–571.

Zhang, C.L., Zhang, G.W., Yan, Y.X., Wang, Y., 2005. Origin and dynamic significance of Guangtoushan granitic plutons to the north of Mianlue zone in southern Qinling. Acta Petrol. Sin. 21, 711–720.

Zhang, G.W., Guo A.L., and Yao A.P. 2004. Western Qinling-Songpan continental tectonic node in China’s continental tectonics, Earth Sci. Front, 11(3), 23–32 (in Chinese with English abstract).Zhang, G.W., Meng, Q.R., Lai, S.C., 1995.

Tectonics and structure of Qinling orogenic belt. Sci. China Earth Sci. 38, 1379–1394.

Zhang, J.Y., Ma, C.Q., Xiong, F.H., Liu, B., 2012. Petrogenesis and tectonic significance of the Late Permian–Middle Triassic calc-alkaline granites in the Balong region, eastern Kunlun Orogen, China. Geo. Mag. 149, 892–908.

Zhao, B.Q., 2010. Characteristics and cause analysis to the north–south fault of Duohemao area in Qinghai province. (Master) China University of Geosciences, Beijing 50.

Zheng, Y.F., Fu, B., Li, Y., Xiao, Y., Li, S., 1998. Oxygen and hydrogen isotope geochemistry of ultrahigh pressure eclogites from the Dabie Mountains and the Sulu terranes. Earth Planet. Sci. Lett. 155, 113–129.

Zhou, G.Z., Gao, J.L., Kang, W.G., Liu, X.C., 1990. Several problems on the blueschist belt in northern Hubei. Regional Geology of China, 3, 255–261 (in Chinese with English abstract).

Zhou, M.F., Zhao, J.H., Jiang, C.Y., Gao, J.F., Wang, W., Yang, S.H., 2009. OIB-like, heterogeneous mantle sources of Permian basaltic magmatism in the western Tarim Basin, NW China: Implications for a possible Permian large igneous province. Lithos 113, 583–594.

Zindler, A., Jagoutz, E., Goldstein, S., 1982. Nd, Sr and Pb isotopic systematics in a three component mantle: a new perspective. Nature 298, 519–523.

Zou, H., Zindler, A., Xu, X.S., Qi, Q., 2000. Major, trace element, and Nd, Sr and Pb isotope studies of Cenozoic basalts in SE China; mantle sources, regional

variations, and tectonic significance. Chem. Geol. 171, 33–47.

Figure Captions

Fig. 1 (a) Simplified geological map of major units in China showing the Qinling orogenic belt (Zheng et al., 2009; Dong et al., 2011). (b) Geological map of the western Qinling orogenic belt (after Feng et al., 2002; Zhang et al., 2006; Li et al., 2013b, 2015; Craddock et al., 2012; Horton et al., 2004). Geological map for the Duofutun (c) and Hongqiang (d) areas showing the Early Cretaceous sequence. The symbols refer to $^{40}Ar/^{39}Ar$ dating sampling locations.

Fig. 2 The hornblende and whole-rock $^{40}Ar/^{39}Ar$ plateau age spectra and $^{40}Ar/^{36}Ar$ versus $^{39}Ar/^{36}Ar$ for the basaltic samples of TR-12B (a and a') and TR-25 (b and b')

Fig. 3 Total alkali versus SiO_2 (TAS) diagram (after Le Maitre, 2002) for the basaltic volcanics in the western Qinling orogenic belt.

Fig. 4. SiO_2 versus major oxides (a–f), and MgO versus Cr (g) and Ni (h). The oxides are normalized to 100 wt.% by volatile-free. The filled circle and square symbols represent the Group1 and Group 2 samples, respectively.

Fig. 5 (a) The patterns of the chondrite-normalized rare-earth elements and (b) primitive mantle-normalized spidergram for the Group 1 and Group 2 samples.

Chondrite- and primitive mantle-normalize values are from Taylor and McLennan (1985) and Sun and McDonough (1989), respectively.

Fig. 6 Sr-Nd isotopic variations of the Early Cretaceous Group 1 and Group 2 samples in the western Qinling orogenic belt. MORB, DM, OIB, HIMU, EMI and EMII fields are from Zindler and Hart (1986); FOZO field is from hart et al. (1992) and Hauri et al. (1994). The field of Cenozoic basalts in eastern China is from Liu et al. (1996) and Zou et al.(2000).

Fig. 7 SiO_2 versus Th/La (a), Nb/La (b), $\varepsilon_{Nd}(t)$ (c) and $^{87}Sr/^{86}Sr_{(i)}$ (d) for the Group 1 and Group 2 samples in the western Qinling orogenic belt.

Fig. 8. Plot of La and La/Sm (a) of the Early Cretaceous mafic samples in the western Qinling orogenic belt. Symbols as in Fig. 3.

Figure

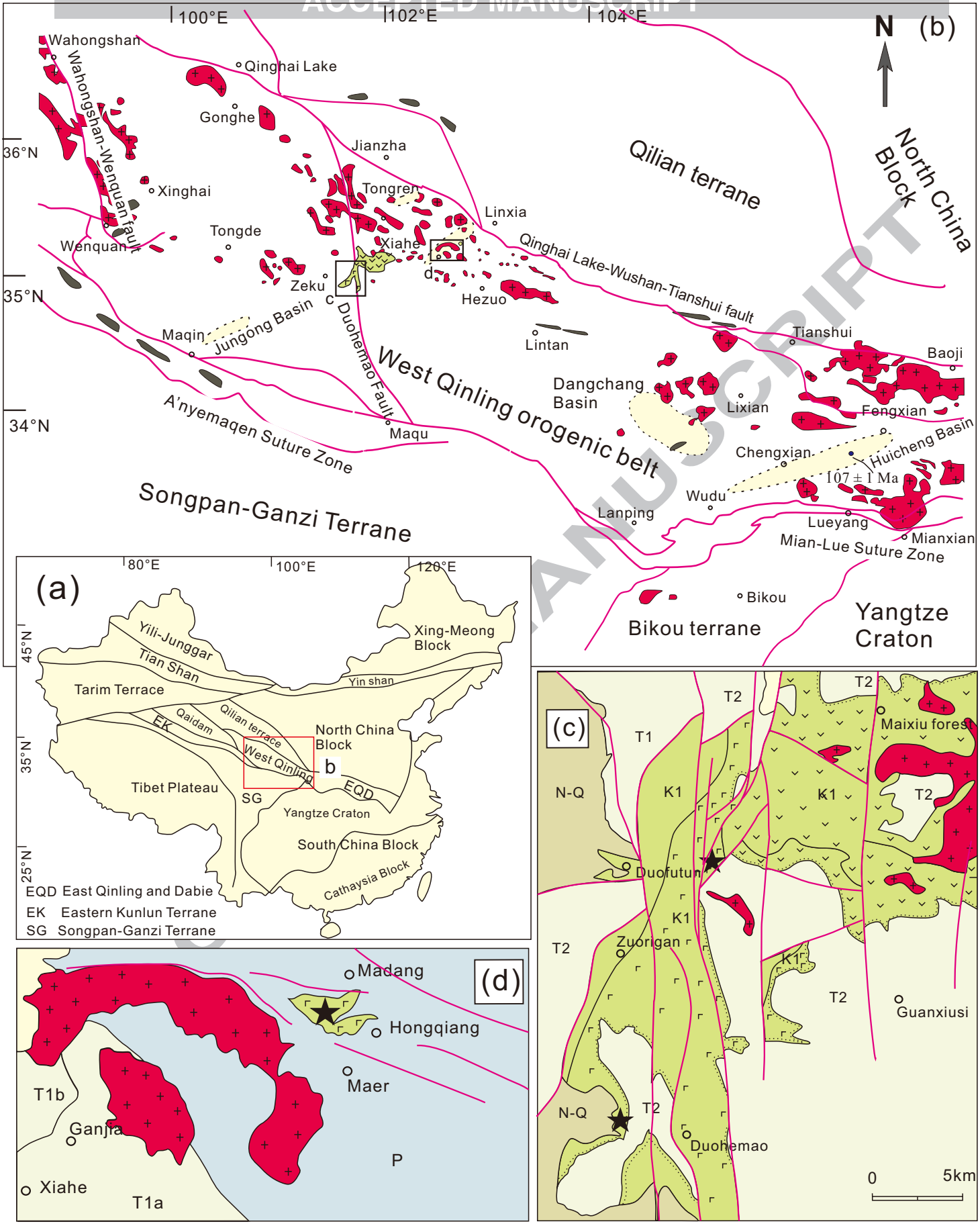

Fig. 1 Zhang F-F and coauthors

Figure

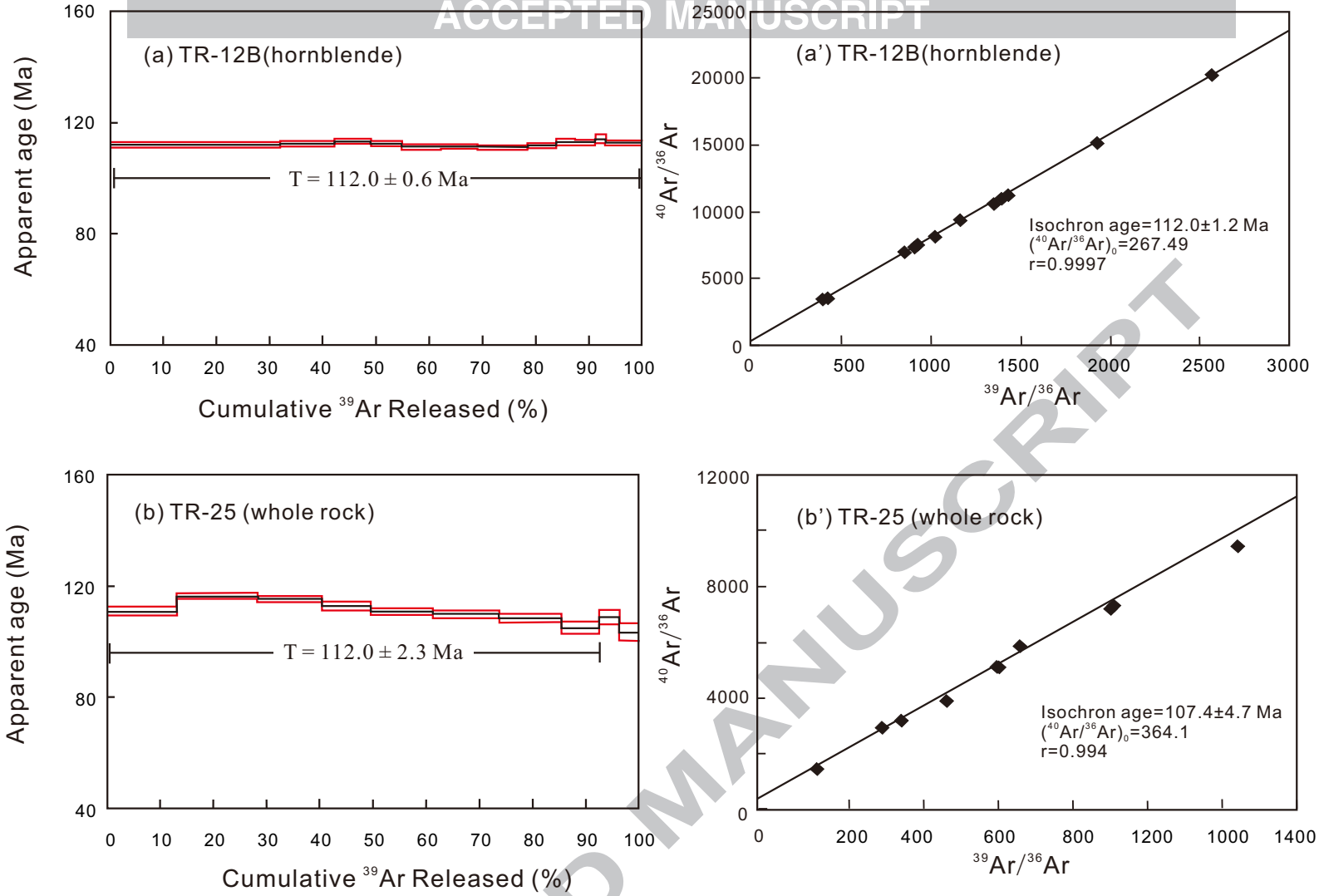

Fig. 2 Zhang FF and coauthors

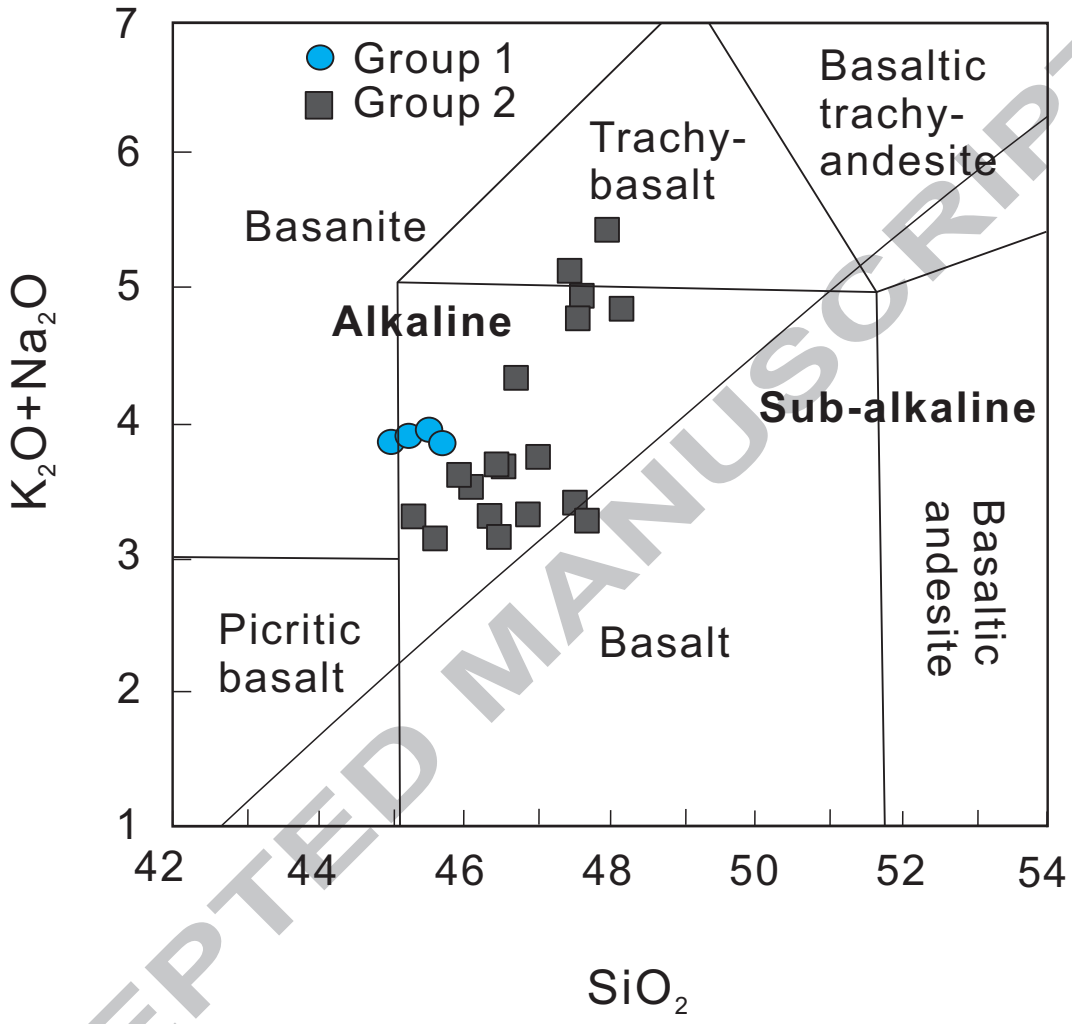

Fig.3 Zhang FF and coauthors

Figure

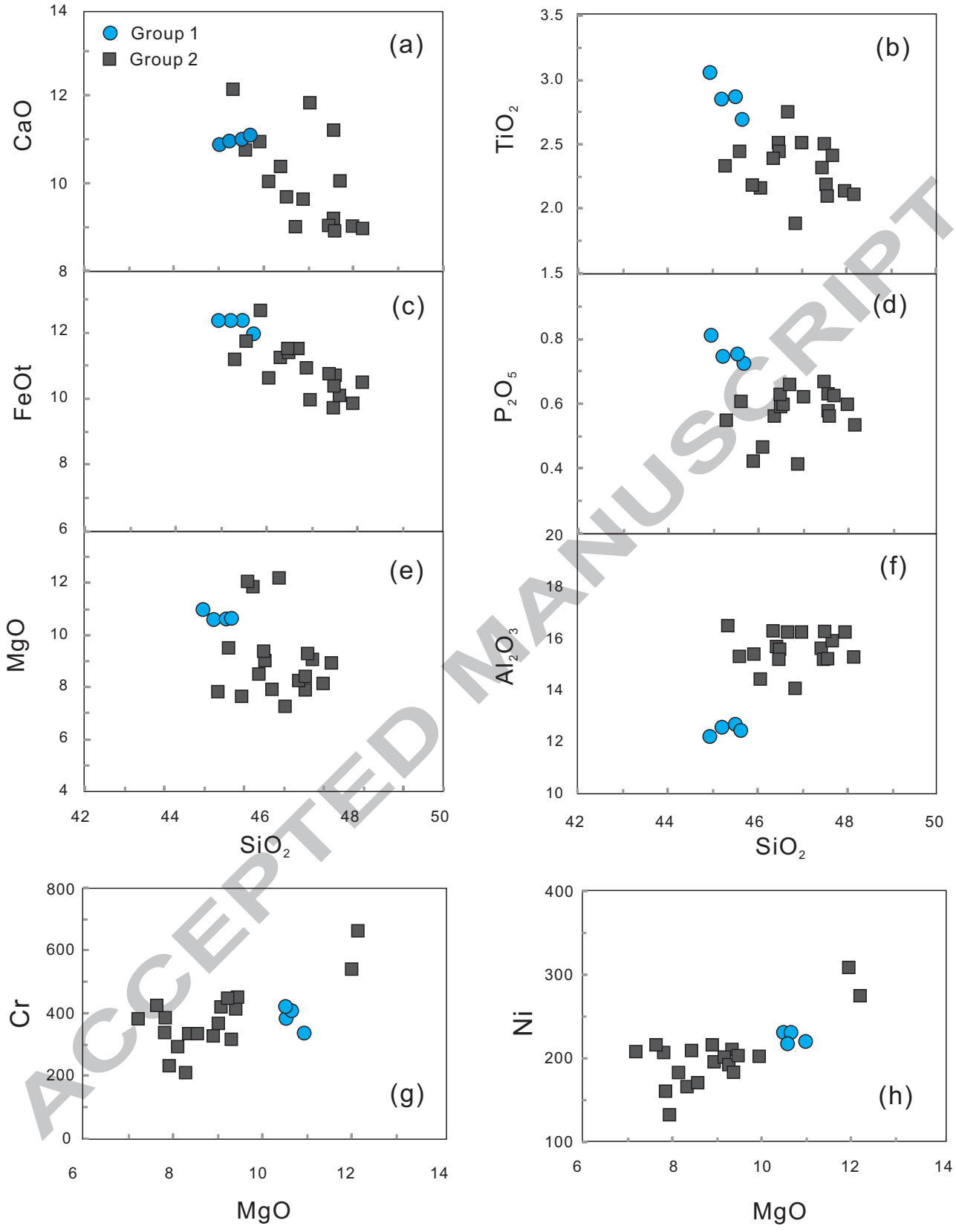

Fig. 4 Zhang FF and coauthors

Figure

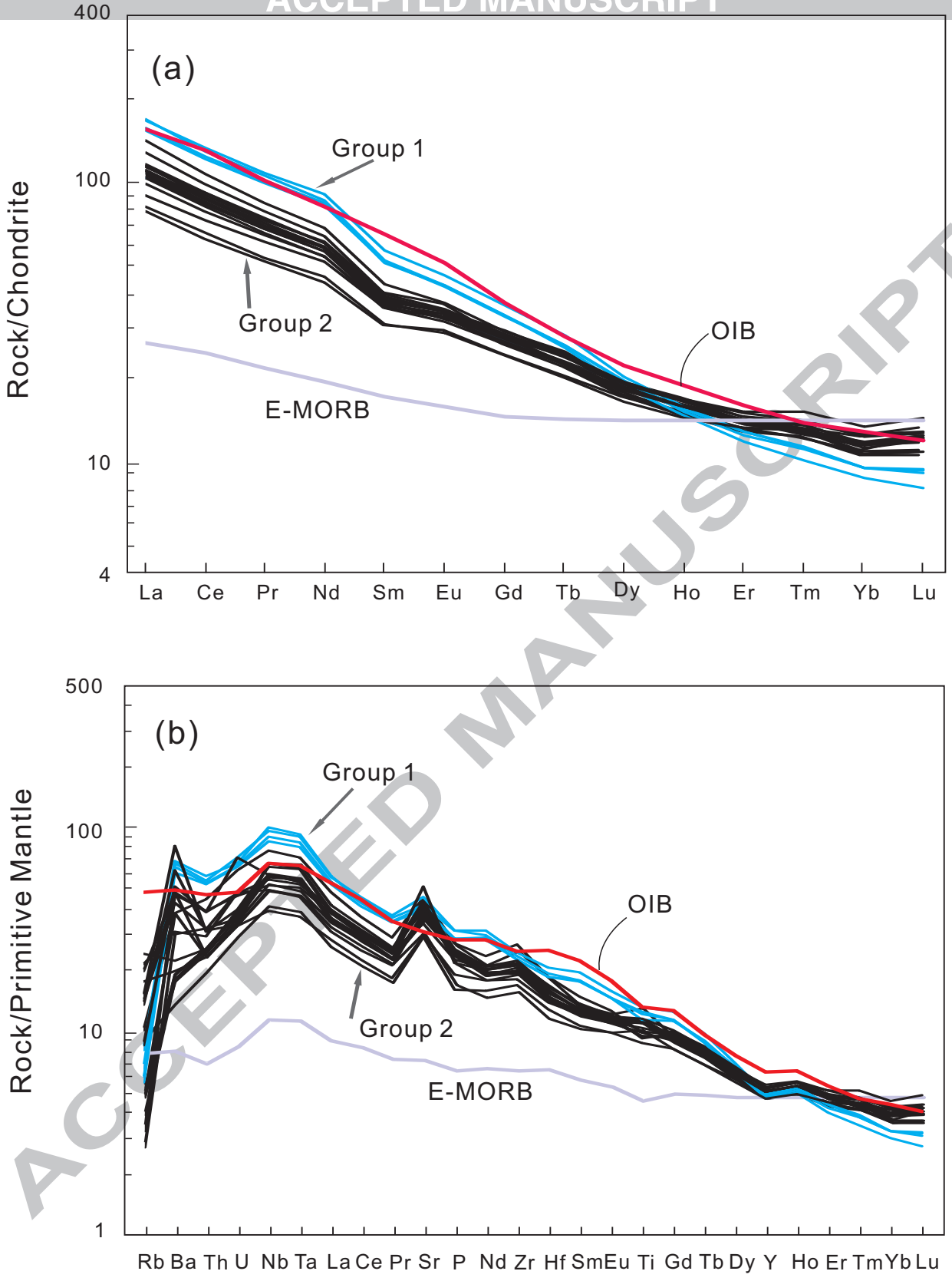

Fig. 5 Zhang FF and coauthors

Figure

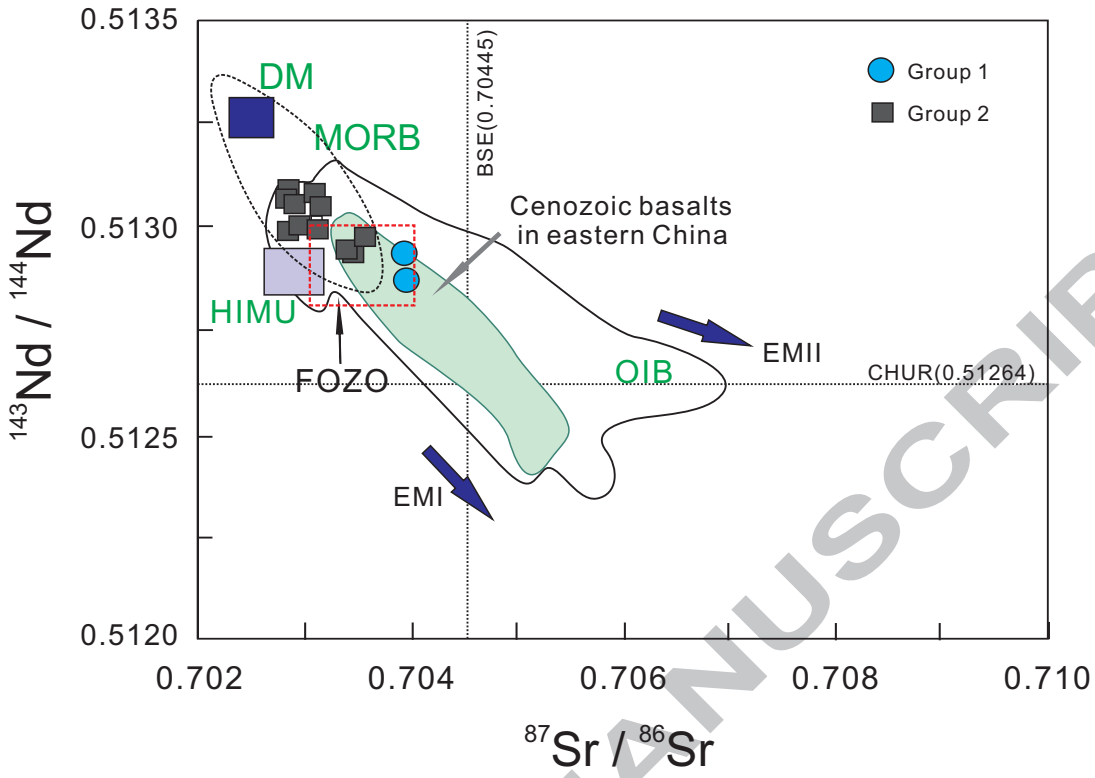

Fig.6 Zhang FF and coauthors

Figure

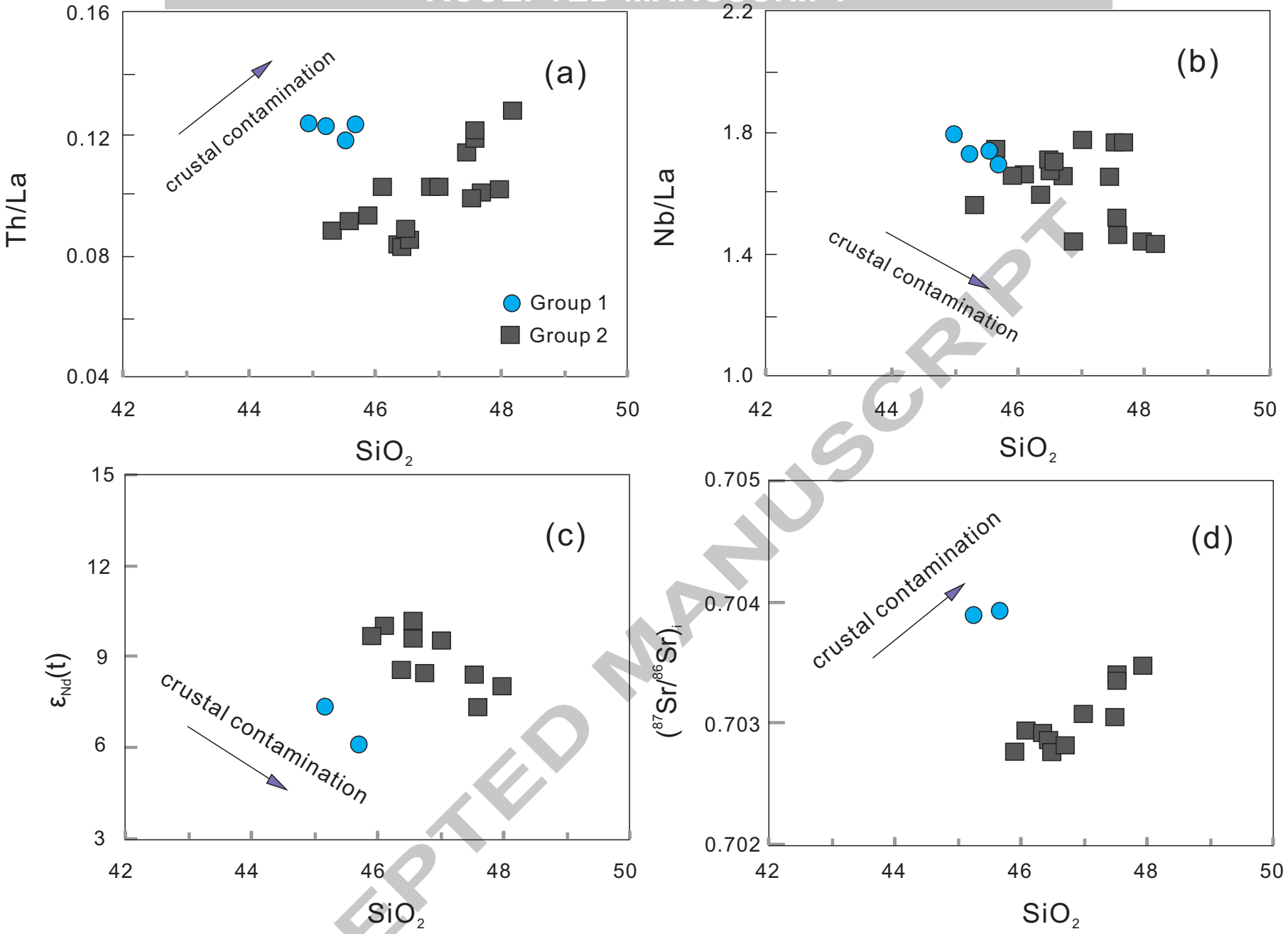

Fig.7 Zhang FF and coauthors

Figure

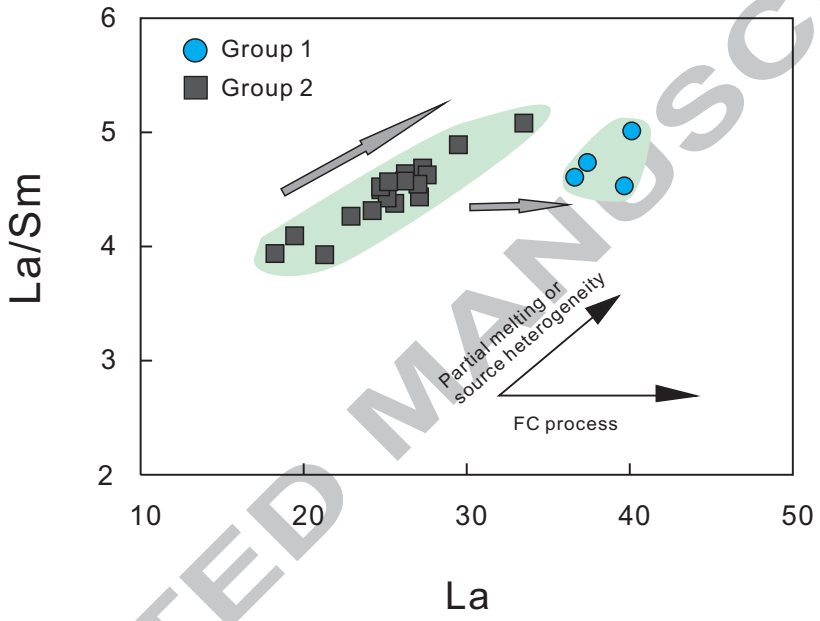

Fig. 8 Zhang FF and coauthors

Table 1 $^{40}Ar/^{39}Ar$ isotopic results of incremental heating experiments for the basaltic rocks from the western Qinling orogenic belt

Temp (W)	$(^{40}Ar/^{39}Ar)_m$	$(^{36}Ar/^{39}Ar)_m$	$(^{37}Ar/^{39}Ar)_m$	$(^{38}Ar/^{39}Ar)_m$	$^{39}Ar_k$ (10^{-12}mol)	$(^{40}Ar^*/^{39}Ar_k)$	±1s	$^{39}Ar_k$ (%)	Apparent age (Ma)	±1s
TR-12(B) hornblende, J=0.008303										
4	8.413	0.00237	1.41181	0.00133	0.0451	7.712	0.029	32.2	111.97	0.81
4.5	8.069	0.00111	1.642	0.00126	0.0141	7.741	0.023	10.1	112.38	0.65
5	7.902	0.00039	1.82163	0.00121	0.0094	7.787	0.029	6.72	113.03	0.81
5.5	7.904	0.00052	2.36228	0.00118	0.0082	7.751	0.029	5.86	112.52	0.81
6.5	7.871	0.00074	2.20331	0.00145	0.0103	7.654	0.024	7.35	111.16	0.69
7.5	7.869	0.0007	2.45932	0.0014	0.0093	7.663	0.025	6.67	111.29	0.69
9	7.854	0.00072	2.19496	0.00123	0.0136	7.642	0.023	9.7	110.99	0.64
11	7.983	0.00098	2.09465	0.00135	0.0075	7.694	0.029	5.36	111.72	0.82
14	8.096	0.00108	1.61209	0.00111	0.0048	7.775	0.039	3.4	112.86	1.09
19	8.116	0.00117	1.89356	0.00122	0.0056	7.77	0.029	4	112.79	0.81
29	8.587	0.0025	0.96009	0.00091	0.0024	7.848	0.057	1.68	113.89	1.6
50	8.017	0.00086	1.15545	0.00116	0.0098	7.761	0.032	6.97	112.67	0.89
Inverse isochron age: 112.0± 0.6 Ma m=0.20g										
TR-25 whole rock, J=0.008168										
5	9.671	0.00646		0.00127	0.0051	7.762	0.056	13.2	110.9	1.55
6.5	8.588	0.00147	0	0.00107	0.0059	8.155	0.037	15.2	116.34	1.03
7.5	8.973	0.00308	0	0.00108	0.0047	8.061	0.044	12.1	115.04	1.21
8.5	8.699	0.0027	0	0.00115	0.0035	7.901	0.061	9.15	112.83	1.69
10	8.218	0.0016	2.52674	0.00145	0.0045	7.745	0.042	11.7	110.67	1.17
11	8.158	0.00161	2.43184	0.00137	0.0049	7.683	0.047	12.6	109.8	1.29
12.5	7.903	0.00109	4.93524	0.0014	0.0045	7.58	0.054	11.7	108.38	1.5
13.5	7.93	0.00204	4.51809	0.00121	0.0027	7.326	0.081	6.94	104.85	2.24
14.5	7.923	0.00108	4.53445	0.00137	0.0015	7.603	0.088	3.89	108.69	2.43
16	7.454	0.0008	5.3433	0.00114	0.0014	7.219	0.106	3.71	103.35	2.94
Inverse isochron age: 112.0±2.3 Ma m=0.20g										

Table 2 Major and trace elemental data of the Early Cretaceous basaltic rocks from the western Qinling orogenic belt

	TR-5	TR-7	TR-9	TR-11	TR-2	TR-3	TR-12(B)	TR-13	TR-15	TR-25	TR-26
Sample	Group 1				Group 2						
SiO_2	44.98	45.70	45.23	45.52	47.97	47.45	47.58	47.55	48.19	47.53	47.02
TiO_2	3.06	2.69	2.85	2.87	2.14	2.32	2.10	2.19	2.11	2.50	2.51
Al_2O_3	12.23	12.49	12.58	12.66	16.27	15.63	15.24	15.22	15.26	16.28	16.23
Fe_2O_3	7.13	6.82	7.01	7.05	3.72	5.29	4.91	4.57	4.54	5.59	5.71
FeO	5.94	5.83	5.96	6.00	6.53	5.96	6.24	6.29	6.38	4.67	4.83
CaO	10.79	11.10	10.94	11.02	9.02	9.03	8.92	9.19	8.98	11.18	11.83
MgO	10.98	10.59	10.58	10.65	8.15	8.33	9.34	8.43	8.93	7.90	7.25
K_2O	0.75	0.63	0.64	0.65	1.58	1.17	1.43	0.93	1.04	0.96	0.98
Na_2O	3.14	3.22	3.26	3.29	3.86	3.96	3.51	3.85	3.84	2.48	2.77
P_2O_5	0.81	0.72	0.75	0.75	0.60	0.67	0.56	0.58	0.53	0.63	0.62
LOI	4.55	2.86	3.25	3.85	2.54	4.19	3.54	3.85	4.17	4.55	4.48
Total	99.69	99.71	99.74	99.71	99.77	99.76	99.76	99.76	99.73	99.74	99.74
mg#	0.42	0.41	0.41	0.41	0.39	0.38	0.40	0.40	0.40	0.31	0.32
Sc	18.6	20.4	20.7	22.2	19.8	20.8	22.5	23.1	22.6	25.0	26.0
Ti	16390	14869	16030	17179	12391	12977	12142	13155	12384	14255	15046
V	466	208	205	225	120	155	162	171	166	187	189
Cr	336	418	381	399	291	208	317	334	329	373	379
Co	51.2	51.2	51.2	51.9	40.1	44.8	47.9	47.3	45.1	47.3	46.4
Ni	221	229	218	231	183	166	208	209	196	207	208
Ga	19.8	19.8	19.4	20.3	15.5	18.6	18.2	18.5	17.6	17.3	18.1
Ge	1.34	1.47	1.42	1.47	1.32	1.35	1.41	1.38	1.39	1.54	1.49
Rb	5.17	3.60	4.18	3.66	13.66	6.45	12.66	5.44	9.52	8.63	8.98
Sr	887	838	867	973	960	956	723	835	1091	928	897
Y	21.6	22.2	22.1	22.7	25.1	23.5	23.2	24.0	23.3	24.0	24.4
Zr	265	254	256	274	231	300	239	250	237	242	246
Nb	71.9	61.9	64.8	69.1	35.6	55.4	39.9	41.9	37.7	48.0	48.0
Ba	485	426	455	474	217	269	341	364	331	434	303
La	40.1	36.6	37.4	39.7	24.7	33.5	27.3	27.6	26.2	27.1	27.0
Ce	78.9	74.1	76.3	81.8	50.2	65.5	54.2	56.5	54.0	55.0	56.0
Pr	10.1	9.5	9.7	10.3	6.3	8.0	6.8	7.1	6.8	7.0	7.1
Nd	40.5	38.5	39.4	42.5	25.4	32.1	27.6	28.5	27.2	28.5	28.4
Sm	8.0	8.0	7.9	8.8	5.5	6.6	5.8	6.0	5.7	6.1	5.9
Eu	2.49	2.47	2.49	2.68	1.90	2.16	2.01	2.00	1.91	2.04	2.00
Gd	6.87	6.80	6.86	7.47	5.57	5.97	5.88	5.80	5.68	5.85	6.05
Tb	0.96	0.97	0.97	1.06	0.85	0.92	0.89	0.89	0.85	0.91	0.91
Dy	4.71	4.88	4.93	5.11	4.80	4.77	4.71	4.81	4.62	4.87	4.92
Ho	0.83	0.87	0.85	0.89	0.94	0.89	0.89	0.92	0.89	0.92	0.93
Er	1.93	2.11	2.04	2.12	2.48	2.25	2.28	2.31	2.32	2.39	2.47
Tm	0.26	0.28	0.28	0.29	0.38	0.32	0.33	0.34	0.35	0.35	0.36
Yb	1.48	1.61	1.61	1.60	2.27	1.80	1.94	1.98	1.93	2.11	2.09
Lu	0.20	0.24	0.24	0.23	0.36	0.27	0.31	0.31	0.31	0.32	0.32

Hf	5.96	5.75	5.79	6.39	4.49	5.77	4.82	5.16	4.92	5.15	5.25
Ta	3.85	3.33	3.50	3.73	1.90	2.97	2.18	2.26	2.10	2.61	2.64
Th	4.95	4.51	4.58	4.69	2.51	3.81	3.30	3.31	3.35	2.68	2.76
U	1.41	1.36	1.38	1.51	1.02	1.30	1.01	1.51	0.98	0.71	0.75
(La/Yb)n	19.48	16.36	16.66	17.80	7.83	13.32	10.07	9.97	9.76	9.20	9.28
(Gd/Yb)n	3.85	3.50	3.53	3.86	2.03	2.74	2.50	2.42	2.44	2.29	2.40
Eu/Eu*	1.03	1.03	1.03	1.01	1.05	1.05	1.05	1.04	1.03	1.04	1.02
	TR-27	TR-28	TR-29	TR-62	TR-64	TR-65	TR-66	TR-68	TR-70	TR-71	TR-72
Sample	Group 2										
SiO_2	47.70	46.11	46.88	46.48	45.91	46.54	45.60	46.71	45.32	46.50	46.37
TiO_2	2.41	2.16	1.88	2.53	2.18	2.45	2.45	2.75	2.33	2.47	2.39
Al_2O_3	15.92	14.41	14.05	15.67	15.44	15.57	15.33	16.28	16.48	15.38	16.32
Fe_2O_3	5.72	3.90	5.06	7.82	9.24	6.65	7.21	5.81	7.48	6.78	7.11
FeO	5.02	7.16	6.41	4.40	4.35	5.42	5.25	6.26	4.44	5.38	4.84
CaO	10.05	10.04	9.62	9.70	10.94	9.68	10.76	9.02	12.14	9.84	10.35
MgO	9.05	12.04	12.19	9.41	7.68	9.19	9.48	7.95	7.85	9.16	8.51
K_2O	0.98	1.47	1.14	0.83	0.87	0.97	0.81	0.64	0.55	0.92	0.51
Na_2O	2.32	2.07	2.19	2.37	2.76	2.72	2.36	3.71	2.73	2.78	2.79
P_2O_5	0.62	0.47	0.41	0.63	0.42	0.60	0.61	0.67	0.55	0.60	0.56
LOI	5.16	3.33	3.03	4.23	3.16	3.86	4.61	3.94	5.07	4.06	3.72
Total	99.71	99.76	99.76	99.77	99.78	99.75	99.78	99.77	99.74	99.76	99.76
mg#	0.33	0.44	0.42	0.31	0.31	0.35	0.35	0.38	0.30	0.35	0.32
Sc	23.8	26.5	25.3	25.3	27.5	25.6	25.1	21.9	28.2	24.2	29.1
Ti	13694	12971	11526	15210	13418	14696	14488	17349	14706	14666	15161
V	174	190	177	187	203	180	180	176	195	179	200
Cr	362	538	663	429	426	440	441	228	338	432	342
Co	47.4	53.8	54.3	46.1	51.6	46.7	48.7	44.7	49.1	47.9	49.2
Ni	216	302	271	188	217	193	203	140	161	202	170
Ga	17.2	16.4	15.9	17.7	17.8	17.3	17.1	18.1	17.3	17.2	18.4
Ge	1.43	1.39	1.32	1.55	1.61	1.49	1.44	1.44	1.43	1.54	1.55
Rb	9.44	15.49	11.20	2.51	5.86	3.43	3.05	1.74	3.15	3.09	2.09
Sr	864	639	622	817	648	762	845	942	855	791	814
Y	23.1	23.3	21.4	22.3	21.7	22.1	21.5	23.4	23.3	22.0	24.4
Zr	237	204	191	228	179	22	224	285	217	222	230
Nb	46.3	35.3	28.0	43.7	30.2	42.7	43.0	48.9	35.9	42.1	38.6
Ba	574	157	140	129	97.1	125	136	216	272	135	348
La	26.2	21.3	19.5	25.6	18.2	25.1	24.7	29.5	22.9	25.2	24.2
Ce	53.6	44.6	40.2	52.6	37.8	50.5	50.0	59.1	47.4	51.1	50.3
Pr	6.7	5.8	5.1	6.5	4.9	6.4	6.3	7.3	6.0	6.4	6.4
Nd	27.3	24.4	21.5	26.9	20.1	26.7	26.0	29.4	24.8	26.7	25.8
Sm	5.7	5.4	4.8	5.8	4.6	5.7	5.5	6.0	5.4	5.5	5.6
Eu	1.87	1.85	1.67	1.97	1.68	1.96	1.94	2.09	1.87	1.92	1.96
Gd	5.75	5.40	4.90	5.60	4.90	5.39	5.36	5.62	5.37	5.51	5.70
Tb	0.84	0.83	0.74	0.84	0.75	0.83	0.81	0.88	0.85	0.83	0.87

Dy	4.66	4.55	4.14	4.61	4.29	4.48	4.31	4.68	4.62	4.37	4.83
Ho	0.89	0.89	0.81	0.87	0.84	0.84	0.81	0.88	0.90	0.85	0.94
Er	2.24	2.29	2.18	2.25	2.17	2.12	2.09	2.28	2.31	2.15	2.36
Tm	0.33	0.33	0.33	0.32	0.33	0.31	0.31	0.32	0.33	0.31	0.35
Yb	1.99	1.98	1.90	1.93	1.85	1.78	1.77	1.91	2.06	1.83	2.08
Lu	0.32	0.31	0.30	0.30	0.31	0.27	0.27	0.29	0.32	0.28	0.33
Hf	4.98	4.33	3.99	4.88	3.64	4.63	4.50	5.75	4.41	4.62	4.67
Ta	2.58	1.89	1.51	2.37	1.62	2.32	2.30	2.78	1.95	2.34	2.06
Th	2.64	2.17	1.99	2.20	1.69	2.14	2.24	2.81	2.02	2.23	2.01
U	0.84	0.70	0.70	0.86	0.63	0.79	0.82	1.07	0.73	0.83	0.76
(La/Yb)n	9.42	7.72	7.35	9.52	7.07	10.12	10.00	11.06	7.97	9.88	8.34
(Gd/Yb)n	2.38	2.26	2.13	2.40	2.19	2.50	2.50	2.43	2.16	2.49	2.27
Eu/Eu*	1.00	1.04	1.06	1.05	1.08	1.08	1.09	1.10	1.07	1.06	1.06

LOI: Loss ion ignition, mg-number=Mg^{2+} /(Mg^{2+} +Fe^{2+}); Reference values of AMH-1 and OU-3 international standard are from Thompson et al. (2000) and Potts et al. (2000).

Table 3 Sr-Nd isotopic composition of early Cretaceous basaltic rocks from the western Qinling orogenic belt

Sample	Sm	Nd	Rb	Sr	$^{147}Sm/^{144}Nd$	$^{143}Nd/^{144}Nd$	$^{87}Rb/^{86}Sr$	$^{87}Sr/^{86}Sr$	$(^{87}Sr/^{86}Sr)_i$	$\varepsilon_{Nd}(t)$
Group 1										
TR-7	7.95	38.52	3.60	838.0	0.125	0.512886±12	0.012	0.703942±11	0.703917	6.13
TR-9	7.90	39.37	4.18	866.9	0.121	0.512950±11	0.014	0.703922±14	0.703894	7.43
Group 2										
TR-2	5.50	25.44	13.66	959.5	0.131	0.512989±12	0.041	0.703553±15	0.703471	8.03
TR-12(B)	5.83	27.57	12.66	723.0	0.128	0.512953±11	0.051	0.703420±17	0.703319	7.37
TR-13	5.96	28.50	5.44	835.1	0.126	0.512951±10	0.019	0.703441±17	0.703403	7.36
TR-25	6.11	28.54	8.63	927.9	0.130	0.513007±12	0.027	0.703106±15	0.703053	8.40
TR-26	5.94	28.35	8.98	897.1	0.127	0.513062±10	0.029	0.703133±14	0.703075	9.53
TR-28	5.42	24.37	15.49	638.5	0.134	0.513094±11	0.070	0.703078±15	0.702938	10.00
TR-64	4.63	20.14	5.86	647.6	0.139	0.513084±13	0.026	0.702818±15	0.702766	9.72
TR-65	5.68	26.72	3.43	761.9	0.128	0.513096±13	0.013	0.702845±17	0.702819	10.15
TR-68	6.03	29.39	1.74	941.8	0.124	0.513003±11	0.005	0.702825±17	0.702815	8.42
TR-71	5.52	26.65	3.09	791.3	0.125	0.513067±11	0.011	0.702888±13	0.702865	9.66
TR-72	5.61	25.82	2.09	814.3	0.131	0.513017±12	0.007	0.702935±17	0.702920	8.55

Chondrite uniform reservoir values, $^{147}Sm/^{144}Nd=0.1967$, $^{143}Nd/^{144}Nd=0.512638$, are used for the calculation. $\varepsilon_{Nd}(t)$ is calculated by assuming 112 Ma for basaltic rocks from the western Qinling orogenic belt. Sm, Nd, Rb and Sr contents: ppm–

Graphic abstract

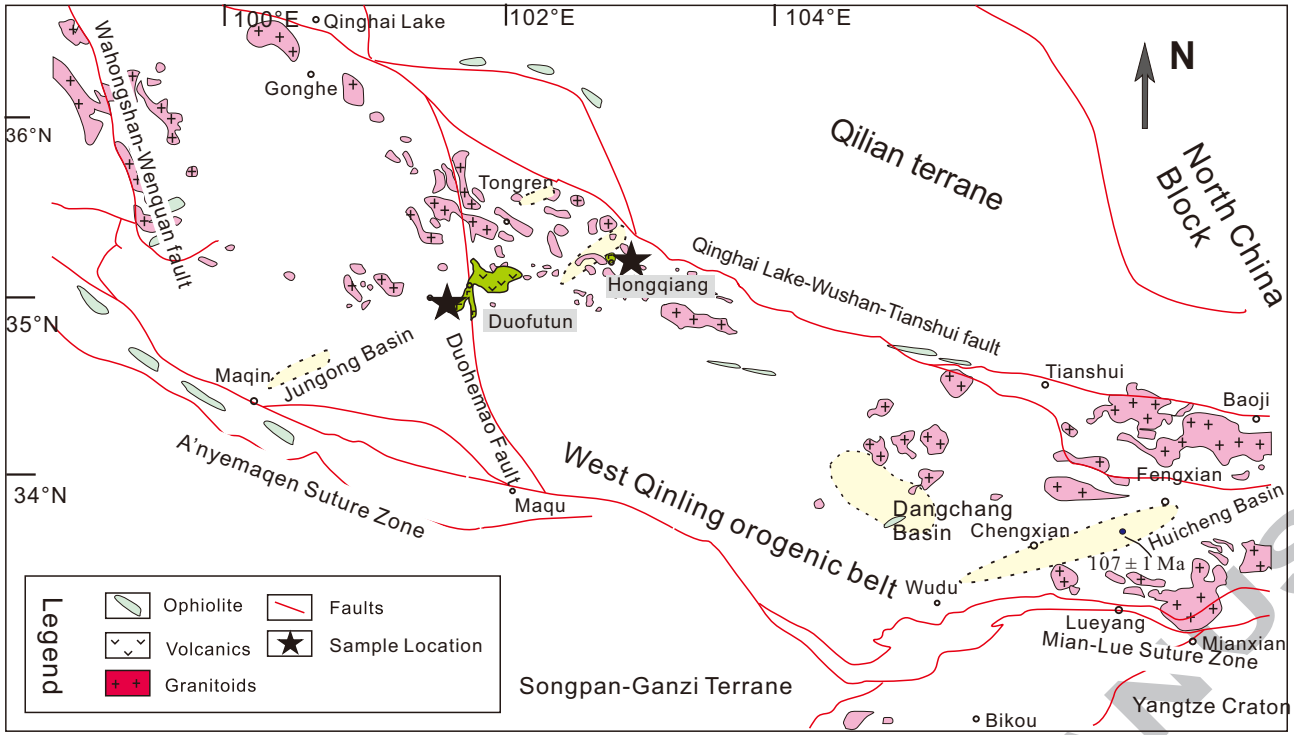

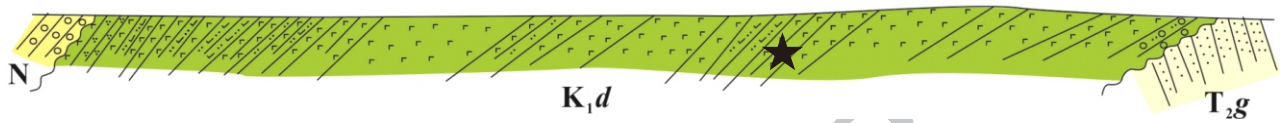

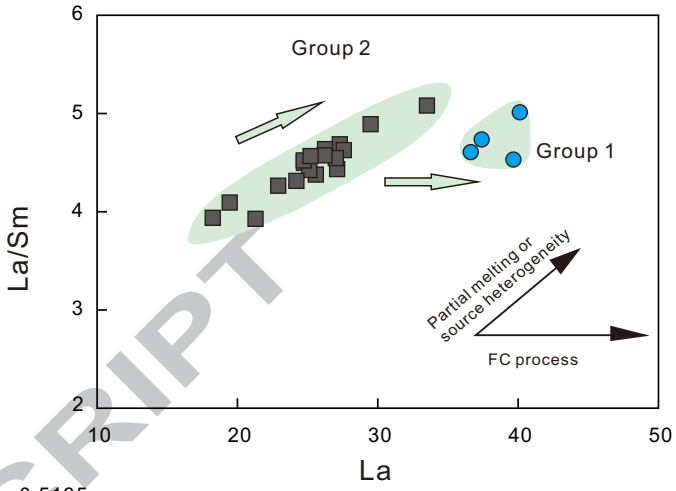

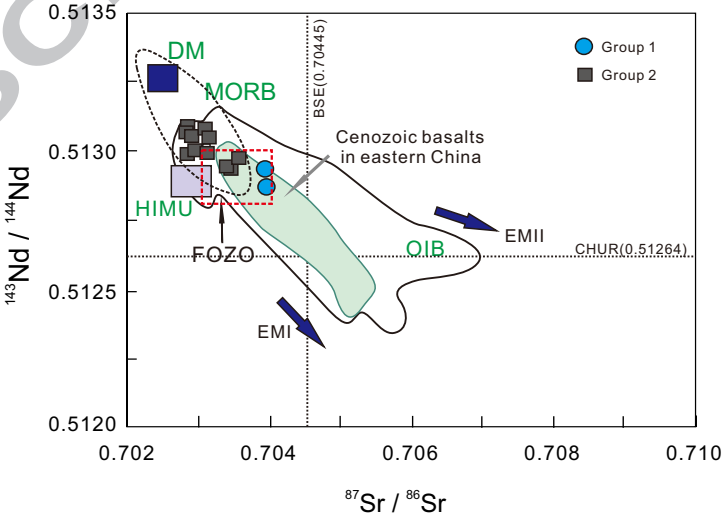

Graphic abstract

Highlights

► Basalts from the western Qinling orogenic belt were erupted at ~112 Ma.

► These basalts were originated from asthenospheric mantle with the lithospheric component

► A petrogenetic model is proposed for Early Cretaceous lithosphere delamination in response to asthenospheric upwelling.